Pattern Recognition 52 (2016) 471–476

Contents lists available at ScienceDirect

Pattern Recognition

journal homepage: www.elsevier.com/locate/pr

# Errata and comments on "Errata and comments on *Orthogonal moments based on exponent functions: Exponent-Fourier moments*"

Hai-tao Hu *, Quan Ju, Chao Shao

*College of Computer and Information and Engineering, Henan University of Economics and Law, Zhengzhou 450002, China*

ARTICLE INFO

*Article history:*
Received 15 February 2015
Received in revised form
2 September 2015
Accepted 8 October 2015
Available online 19 October 2015

*Keywords:*
Orthogonal moments
Radial function
Image recognition
Exponent–Fourier moments

ABSTRACT

In this paper, we demonstrate that Improved Exponent–Fourier moments mentioned in Xiao et al. (2015) [1] are with crucial mistakes in its definition, an image cannot be decomposed and reconstructed by these incorrect Improved Exponent–Fourier moments. The corrected definition of Improved Exponent–Fourier moments is thus given in this paper to solve problems about numerical instability involved in the process of calculating the Exponent–Fourier moments and values of radial functions approach infinity at origin. Experimental results show the superiority of the corrected Improved Exponent–Fourier moments.



## 1. Comment on [1]

Image moments and their nonlinear combinations can be used as global features in pattern recognition. However, non-orthogonal image moments are sensitive to noise and have high redundancy of information. And it is difficult to reconstruct an image by using them, such as geometric moments and rotational moments. To solve these problems, image moments based on polynomials are proposed, such as Zernike moments, pseudo-Zernike [2,3], orthogonal Fourier–Mellin moments [4], Chebyshev–Fourier moments [5] and Jacobi–Fourier moments [6]. However, polynomials, especially higher order polynomials have very high cost of computation, which limits these moments to be applied in practice. In 2003, Radial Harmonic Fourier moments [7] based on Trigonometric functions are introduced. Radial Harmonic Fourier moments have stronger ability in describing images and have much less complexity than image moments based on polynomials. In Ref. [8], Orthogonal moments based on exponent functions Exponent–Fourier moments (EFM) are proposed. EFMs are able to achieve even better overall performance than Radial harmonic Fourier moments in image analysis.

Bin Xiao et al. recently improved the performance of Exponent–Fourier moments by using their Improved Exponent–Fourier moments (IEFM). IEFMs used in Ref. [1] avoid two issues in the process of calculating EFMs: (1) the value of EFMs approaches infinity at the origin; (2) the numerical instability caused by values of radial function approaching infinity in the neighborhood of the origin. The definition of IEFMs in Ref. [1] is defined as follows:

$$I_{nm}=\frac{1}{2\pi a_n}\int_{\pi}^{\pi+1}\int_{0}^{2\pi} f(r,\theta)T_n(r)\exp(-jm\theta)r\,dr\,d\theta \tag{1}$$

$$T_n(r)=\sqrt{\frac{1}{r}}\exp(-j2\pi nr) \tag{2}$$

Where $f(r,\theta)$ is an original image, $a_n=\exp(-j4n\pi^2)$ is the normalization constant, $n,m=0,\pm1,\pm2,\pm3,\ldots$ are the moment orders, $T_n(r)$ is the radial function.

The orthogonality of $T_n(r)$ is proved in the Ref. [1] over the interval $[\pi,\pi+1]$: Let $r=\pi+r'$, we have $dr=dr'$, and $T_n(r)$ satisfies Eq. (1), so the $T_n(r)$ is orthogonal:

$$\begin{aligned}\int_{\pi}^{\pi+1} T_n(r)T_m(r)r\,dr &= \int_0^1 \sqrt{\frac{1}{\pi+r'}}\exp(-j2n\pi(\pi+r'))\\ &\quad\cdot\sqrt{\frac{1}{\pi+r'}}\exp(-j2m\pi(\pi+r'))(\pi+r')\,dr'\\ &=\exp(-j2n\pi^2)\exp(-j2m\pi^2)\int_0^1\exp(-j2n\pi r')\\ &\quad\cdot\exp(j2m\pi r')\,dr'=\exp(-j4n\pi^2)\delta_{nm}\end{aligned} \tag{3}$$

In Ref. [1], authors try to solve the issue mentioned above during the computation by translating the integral interval from $(0,1]$ to $[\pi,\pi+1]$. However, in the process of EFMs calculating, the original image is first normalized into a unit circle. As a result, radial coordinates of the normalized image are in the range [0,1], not in $[\pi,\pi+1]$. In another words, there is no

* Corresponding author.

http://dx.doi.org/10.1016/j.patcog.2015.10.005
0031-3203/

pixel in the interval $[\pi, \pi+1]$. Using Eq. (3) to calculate EFMs is meaningless.

Moreover, the proof about the orthogonality of $T_n(r)$ in Ref. [1] is not correct. If the function system $T_n(r)$ is orthogonal, the $T_n(r)$ must satisfy Eq. (4), not Eq. (3)

$$\int_{\pi}^{\pi+1} T_k(r)[T_l(r)]^* r\, dr = \delta_{kl} \tag{4}$$

Where $[T_l(r)]^*$ is the complex conjugate of $[T_l(r)]$, $\delta_{kl}$ is the Kronecker symbol. This mistake results in that IEFMs mentioned in Ref. [1] are based on wrong normalization constant $a_n$. Hence, an image can not be decomposed by the function system $[T_n(r)]\exp(-jm\theta)$. Thereby EFMs can not be computed according Eq. (1), As a result, the image also can not be reconstructed by using values of IEFMs computed from Eq. (1) (Reconstructed images in Ref. [1] are incorrect obviously, the correct reconstructed images are shown in Fig. 3 in this paper.). The correct definition of IEFMs is given and discussed with details in the Section 2.

## 2. The corrected definition of the Improved Exponent–Fourier moments (IEFMs)

To avoid the issues mentioned above involved in the process of calculating EFMs, we improve the EFMs by the translating pixels of the normalized image. The improvement version of EFM is as follows:

$$IE_{nm} = \frac{1}{2\pi}\int_{k}^{k+1}\int_{0}^{2\pi} f(r-k,\theta)T_n(r)\exp(-jm\theta)r\, dr\, d\theta \tag{5}$$

Where $k$ is a non-negative integer, $f(r-k,\theta)$ is the translation version of original image $f(r,\theta)$.

**Lemma 1.** *Radial functions $T_n(r)$ of IEFMs are orthogonal over the interval $[k, k+1]$. The proof is listed as follows:*

$$\int_{k}^{k+1} T_n(r)[T_m(r)]^* r\, dr = \int_{k}^{k+1} \sqrt{\frac{1}{r}}\exp(-j2n\pi r) \times \sqrt{\frac{1}{r}}\exp(j2m\pi r) r\, dr = \int_{k}^{k+1} \exp(-j2n\pi r) \cdot \exp(j2m\pi r)\, dr = \delta_{nm} \tag{6}$$

As same as Exponent–Fourier moments [8], an image can be reconstructed approximately using finite series of IEFMs

$$\widehat{f}(r-k,\theta) \approx \sum_{n=1}^{n_{\max}}\sum_{m=1}^{m_{\max}} IE_{nm}[T_n(r)]^*\exp(jm\theta) \tag{7}$$

Compared with the original image, pixels of the reconstructed image from Eq. (7) are shifted a distance $k$ along the radial axis. Pixels of the reconstructed image also must be shifted a distance $k$ along the opposite direction. Figs. 1 and 2 show the real parts of radial function $T_n(r)$ of EFMs and IEFMs with order $n = 0, 1, 2, 3, 4, 5$ respectively. From Figs. 1 and 2, we can find that the radial functions of IEFMs have obviously avoided problems of numerical instability caused by EFMs.

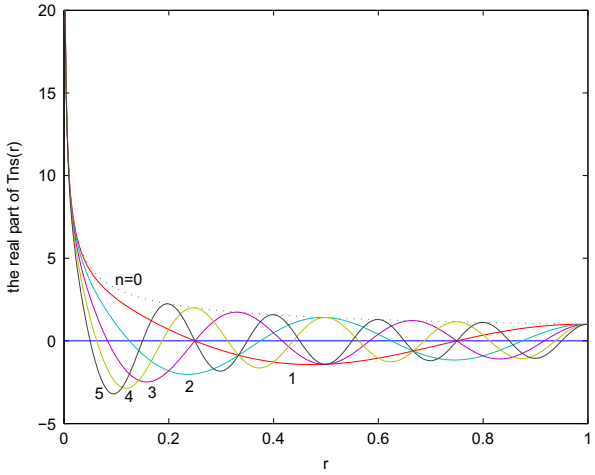


**Fig. 1.** Real parts of radial function $T_n(r)$ of EFMs with $n = 0, 1, 2, 3, 4, 5$.

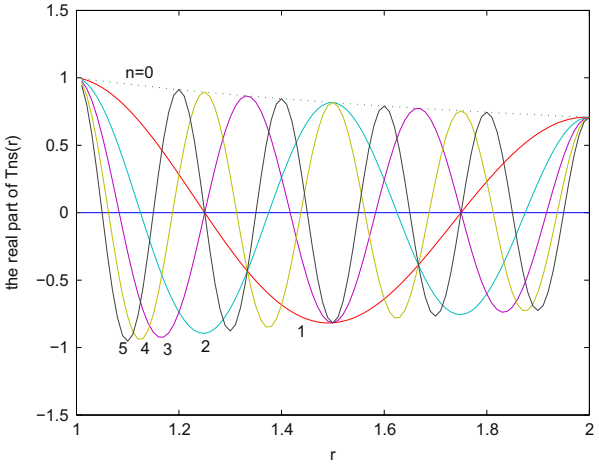


**Fig. 2.** Real parts of radial function $T_n(r)$ of IEFMs with $n = 0, 1, 2, 3, 4, 5$ and $k = 1$.

## 3. Experimental results

Experiments of image reconstruction are provided in this section to verify our proposed method.

*Experiment* 1: An uppercase English letter image "E" is used for testing and its size is $64 \times 64$. We use the mean square reconstruction error (MSRE) used in Ref. [8] to measure the performance of the reconstruction.

All moments from $(1-n_{\max})$ orders are used in the reconstruction. Fig. 3 shows the mesh plots of the reconstructed image by using EFMs and IEFMs with the maximum moment order $n_{\max} = m_{\max} = 25.30$. As can be seen from this figure, these reconstructed images by using IEFMs show more resemblance to their original images than images using EFMs. EFMs produce more reconstruction errors than IEFMs especially when $r$ is close to 0 (at the center of the image). This is because EFMs become numerical unstable during the computation of moments. The MSRE plots of the image "E" are shown in Fig. 4.

*Experiment* 2: Images in the well-known MNIST database are used as the original images in this experiment. These images are then reconstructed with EFMs and IEFMs respectively. MSRE values of the reconstructed images are listed in Table 1. Figs 5 and 6 show MSRE plots of figures "0"–"9". As shown in Table 1, Figs. 5 and 6, these reconstructed images by using IEFMs have much less MSRE values than those by using EFMs except the figure "0". Reconstructed images of figure "0" by using both methods